GMR
The Original

FABRICATION OF SUSTAINABLE CUO NANOPARTICLES LOADED MULTISCALE POLYMERIC ELECTROSPUN NANOSCAFFOLDS FROM *POCOCKIELLA VARIEGATA* EXTRACT FOR POTENTIAL ANTIDIABETIC ACTIVITY

Mathangi Vinayakar Senthilkumar[1], Sai Shiva Ram Meda[2], Santhosh Kumar Thangamani[3], Saranya Natarajan[4], Anguchamy Veeruraj[5*]

[1]Saveetha Medical College & Hospital (SMCH), Saveetha Institute of Medical and Technical Sciences (SIMATS), Thandalam, Chennai, Tamil Nadu 602105, India. Email: mathangivs03@gmail.com
[2]Department of Dermatology, Saveetha Medical College and Hospital, Saveetha Institute of Medical and Technical Sciences (SIMATS), Thandalam, Chennai-602105, Tamil Nadu, India. Email: medasaishivaram@gmail.com Orcid ID: https://orcid.org/0009-0002-2827-6423
[3]Department of Pediatrics, Saveetha Medical College and Hospital, Saveetha Institute of Medical and Technical Sciences (SIMATS), Thandalam, Chennai-602105, Tamil Nadu, India. Email: santhoshdnbmbbs@gmail.com
[4]Department of Biotechnology, Nehru Arts and Science College, Coimbatore-641105, Tamil Nadu, India. Email: nascsaranya.n@nehrucolleges.com
[5*]Saveetha Institute of Basic Medical Sciences (SIBMS), Saveetha Medical College and Hospital, Saveetha Institute of Medical and Technical Sciences (SIMATS), Saveetha University, Chennai, 602 105, Tamil Nadu, India. Email: anguveeruraj@gmail.com Orcid ID : https://orcid.org/0000-0001-7456-6507

ABSTRACT:
This study presents an eco-friendly approach for synthesizing copper oxide nanoparticles (CuO NPs) using Pocockiella variegata marine macroalgae extract via ultrasonic-assisted green synthesis, followed by their incorporation into starch/polyvinyl alcohol (PVA) electrospun nanoscaffolds for enhanced antidiabetic applications. The macroalgal extract served as a reducing and stabilizing agent, facilitating the formation of crystalline CuO NPs, as confirmed by XRD. FTIR spectroscopy revealed the presence of bioactive phytochemicals that capped the nanoparticles, while SEM analysis demonstrated uniform, bead-free nanofibers (150–300 nm) with well-dispersed CuO NPs. The nanoscaffolds exhibited enhanced thermal stability, with degradation delayed up to 362°C, as evidenced by TGA. Antidiabetic efficacy was evaluated through in vitro α-amylase and α-glucosidase inhibition assays. The CuO NPs-loaded nanoscaffolds exhibited superior enzyme inhibition, comparable to the standard drug acarbose, outperforming both the algal extract and standalone CuO NPs. This enhanced activity is attributed to the synergistic effects of phytochemicals, CuO NPs, and the polymeric matrix, which likely facilitate sustained bioactive release. The study highlights the potential of these biocompatible nanoscaffolds as a multifunctional platform for diabetes management, combining structural stability, thermal resistance, and potent antidiabetic properties. Future research should focus on in vivo validation to assess clinical applicability.

KEYWORDS: *Pocockiella variegata*; Green synthesis; CuO nanoparticles; Starch/PVA/CuO-NPs nanoscaffolds; Antidiabetic activity.

1. INTRODUCTION

BThe increasing prevalence of diabetes mellitus worldwide has necessitated the development of novel therapeutic strategies that are not only effective but also environmentally sustainable and biocompatible [1]. Conventional antidiabetic drugs, while effective, often come with side effects and high costs, prompting researchers to explore alternative approaches [2]. In recent years, nanotechnology has emerged as a promising field for biomedical applications, particularly in drug delivery and disease management [3]. Among various nanomaterials, copper oxide nanoparticles (CuO NPs) have gained significant attention due to their unique physicochemical properties, including high surface area, catalytic activity, and biocompatibility [4]. However, the conventional chemical synthesis of CuO NPs often involves toxic reducing agents and generates hazardous byproducts, raising environmental and safety concern [5]. This has led to a growing interest in green synthesis methods that utilize natural extracts as reducing and stabilizing agents, offering an eco-friendly and sustainable alternative [6].

Marine macroalgae, such as Pocockiella variegata, are rich sources of bioactive compounds, including polyphenols, flavonoids, and polysaccharides, which can facilitate the reduction of metal ions and stabilize nanoparticles [7]. The use of macroalgal extracts for nanoparticle synthesis not only enhances the biocompatibility of the resulting NPs but also imparts additional biological activities due to the presence of phytochemicals [8]. Ultrasonic-assisted extraction is particularly advantageous as it enhances the release of bioactive compounds from algal biomass through cavitation effects, leading to more efficient nanoparticle synthesis [9]. Furthermore, the integration of these green-synthesized CuO NPs into polymeric nanoscaffolds can provide a controlled and sustained release platform, enhancing their therapeutic efficacy [10].

Electrospinning is a versatile technique for fabricating nanofibrous scaffolds with high surface area, porosity, and tunable mechanical properties [11]. Starch and polyvinyl alcohol (PVA) are widely used biopolymers for electrospinning due to their biocompatibility, biodegradability, and ease of processing [12]. Starch, a natural polysaccharide, offers excellent film-forming properties, while PVA provides mechanical strength and flexibility [13]. The combination of these polymers with CuO NPs can result in nanoscaffolds with enhanced functional properties, including improved thermal stability, mechanical strength, and bioactive release profiles [14]. Such scaffolds are particularly promising for antidiabetic applications, as they can inhibit key carbohydrate-digesting enzymes like α-amylase and α-glucosidase, thereby regulating postprandial blood glucose levels [15].

The antidiabetic potential of CuO NPs and their composites has been explored in recent studies [16], but the combination of green-synthesized CuO NPs with starch/PVA nanoscaffolds remains underexplored [17]. This study aims to bridge this gap by developing an ultrasonic-assisted green synthesis method for CuO NPs using Pocockiella variegata extract [18] and incorporating them into starch/PVA electrospun nanoscaffolds [19]. The objectives of this research include (1) optimizing the green synthesis of CuO NPs using macroalgal extract [20], (2) fabricating and characterizing starch/PVA nanoscaffolds loaded with CuO NPs [17], and (3) evaluating the antidiabetic activity of the resulting nanocomposites through in vitro enzyme inhibition assays [21].

The rationale behind this study lies in the synergistic potential of macroalgal phytochemicals, CuO NPs, and polymeric nanoscaffolds [22]. The phytochemicals in the algal extract not only facilitate the synthesis of CuO NPs but may also contribute to their antidiabetic activity [23]. The incorporation of these NPs into starch/PVA nanoscaffolds can enhance their stability and controlled release, while the nanofibrous structure provides a high surface area for interaction with target enzymes [24]. This multifunctional approach could lead to the development of a biocompatible and sustainable antidiabetic platform with improved efficacy and reduced side effects compared to conventional therapies [25].

Preliminary studies have shown that green-synthesized metal nanoparticles exhibit significant enzyme inhibitory activity [26], but their incorporation into nanofibrous scaffolds for enhanced delivery and stability has not been thoroughly investigated [27]. This study builds on existing knowledge by combining the advantages of green synthesis, electrospinning, and nanotechnology to create a novel antidiabetic material. The use of Pocockiella variegata, a marine macroalga, as a reducing agent is particularly innovative, as it leverages the untapped potential of marine resources for biomedical applications [28]. Additionally, the ultrasonic-assisted extraction method ensures higher yield and efficiency compared to traditional extraction techniques [29].

The characterization of the synthesized CuO NPs and nanocomposite scaffolds were involved advanced techniques such as UV-Visible spectroscopy, FTIR, XRD, SEM, TGA, and zeta potential analysis [30]. These analyses were provided comprehensive insights into the optical properties, functional groups, crystallinity, morphology, thermal stability, and colloidal behavior of the materials. The antidiabetic activity were assessed through in vitro α-amylase and α-glucosidase inhibition assays, with acarbose as a positive control [31]. These results were statistically analyzed to determine the significance of the observed effects and to establish structure-activity relationships [32].

This research is expected to contribute significantly to the fields of nanotechnology, green chemistry, and diabetes management. The development of a biocompatible, eco-friendly, and effective antidiabetic nanomaterial could pave the way for future clinical applications. Moreover, the methodology and findings of this study could be extended to other therapeutic areas, such as wound healing, antimicrobial therapy, and tissue engineering. By addressing the limitations of conventional synthesis methods and drug delivery systems, this study aligns with the global shift toward sustainable and patient-friendly healthcare solutions.

2.MATERIALS AND METHODS

2.1. Materials

The materials utilized for this experimental study included the macroalgae Pocockiella variegata, which was collected from the coastal waters of Rameswaram in Tamil Nadu, India. Copper(II) sulfate pentahydrate ($CuSO_4 \cdot 5H_2O$), obtained from Sigma-Aldrich, was employed for synthesizing CuO NPs. PVA with a molecular weight of 115,000 served as the polymer base during the electrospinning process, and starch procured from a local vendor was incorporated into the nanofiber structure. Analytical-grade reagents and solvents—such as Milli-Q water, ethanol, and other essential chemicals—were sourced from Merck and Sigma-Aldrich. The electrospinning process was carried out using a high-voltage system (HOLMARC HO-NFES-040) combined with a syringe pump to form PVA/CuO NPs nanofibers. Characterization involved instruments such as a UV-Vis spectrophotometer (VIS SPEC V-730), FTIR (Spectrum Two, PerkinElmer), X-ray diffractometer (Bruker D8 Advance), and a scanning electron microscope (SEM JSM-IT800 NANO). The nanoparticle zeta potential and size were assessed via Malvern Zetasizer Ultra, and thermal analysis was done using the PerkinElmer TGA 8000 system. For biological assays, antidiabetic analysis were done.

2.2. Marine Macroalgae Collection

Specimens of Pocockiella variegata macroalgae were harvested from the seashore region of Rameswaram, Tamil Nadu, India. The collected Pocockiella variegata was taxonomically identified and authenticated by Dr V. Veeragurunathan, CSIR-CSMCRI-Marine Algal Research Station, Mandapam Camp 623519, Tamil Nadu, India. A voucher specimen was prepared and deposited at the Herbarium of the CSIR-CSMCRI-Marine Algal Research Station, under the accession number: SI–2025–RMM–024. This authentication ensures botanical accuracy and standardization of the study material. Later, the samples underwent preliminary cleaning with tap water to eliminate debris and adhered particles, followed by multiple rinses using distilled water for further purification. Approximately 100 grams of this cleaned macroalgae were manually cut into small pieces and allowed to air dry at room temperature for two weeks. Once fully desiccated, the biomass was pulverized into a fine powder using a mechanical grinder, which was then stored appropriately for subsequent experimental steps.

2.3. Ultrasonic-Assisted Extraction

Two grams of finely powdered Pocockiella variegata were combined with 50 mL of Milli-Q water in a 100 mL beaker for the extraction process. This mixture underwent sonication in a LABQUEST ultrasonic bath (Borosil, Serial No. 941032329018) at a constant 60°C for a total of 45 minutes to facilitate the release of bioactive substances. Post-sonication, the solution was filtered through Whatman No. 1 filter paper under sterile conditions to remove particulates. The clear filtrate was collected into a sterile 50 mL beaker and stored at 10°C for future analysis. The aqueous extract was also freeze-dried using a lyophilizer to obtain a powdered form for downstream applications [33].

2.4. Green Synthesis of CuO NPs

To biosynthesize CuO NPs, 50 mL of a 0.1 M copper sulfate pentahydrate ($CuSO_4 \cdot 5H_2O$) solution was combined with 10 mL of the algal extract (10 mg of dry extract dissolved in 10 mL of Milli-Q water), maintaining a 5:1 volume ratio. The mixture was stirred continuously at 650 rpm and kept at 60°C for two hours using a magnetic stirrer. The development of a pale bluish-green hue from the original blue solution signified nanoparticle formation. The resulting suspension was washed thrice with distilled water under the same temperature and stirring conditions to remove impurities. Finally, the purified product was subjected to freeze-drying for 48 hours to yield powdered CuO NPs for characterization and further application [34].

2.5. Fabrication of Starch/PVA Electrospun Scaffolds Loaded with CuO NPs

A 15% (w/w) solution of PVA was prepared in distilled water to fabricate electrospun nanofibers. To this solution, 100 mg of starch and an equal quantity of green-synthesized CuO NPs were added, followed by rigorous stirring at 50°C for 2.5 hours to achieve uniform dispersion. Electrospinning was performed using a HOLMARC HO-NFES-040 unit equipped with an HMPSKV30 power supply (0–30 kV, 0.5 mA). The polymer mixture was drawn into a syringe fitted with a 0.84 mm internal diameter needle. Electrospinning conditions were optimized at 11.5 kV applied voltage, a 12.3 cm needle-to-collector distance, and a feed rate of 0.4 mL/h. The fibers were collected on an aluminum foil-covered collector for 6–8 hours under ambient conditions to produce homogenous nanofibrous scaffolds [35-37].

2.6. Physicochemical Characterization

2.6.1. UV–Visible Spectroscopy

The optical characteristics of the macroalgae extract, CuO NPs, and CuO NP-loaded starch/PVA nanofibers were assessed using UV–Visible spectrophotometry. A VIS SPEC V-730 spectrophotometer was employed for scanning absorbance between 200 nm and 800 nm. Deionized water was used as the blank for all spectral measurements, ensuring accurate determination of peak absorbance associated with the nanomaterials [38].

2.6.2. Fourier Transform Infrared (FT-IR) Spectroscopy

FT-IR spectroscopy was conducted using the Spectrum Two (PerkinElmer) system in ATR mode to identify functional groups. Spectral data were obtained for the macroalgal extract, biosynthesized CuO NPs, and the CuO NP-starch-PVA composite scaffolds. The measurement range extended from 4000 to 400 cm^{-1}, with a resolution of 4 cm^{-1}. Each sample scan was repeated 64 times to enhance the signal-to-noise ratio and ensure reproducible molecular fingerprinting for compound interaction analysis [39].

2.6.3. X-ray Diffraction (XRD) Analysis

The crystalline phases present in the synthesized CuO NPs and CuO NP-integrated nanofibers were determined using XRD. The Bruker D8 Advance diffractometer, with CuKα radiation (λ = 1.5406 Å), operated at 40 kV and 40 mA, recorded the patterns. Scanning was performed over a 2θ range from 5° to 90° at a step interval of 0.029649°, which allowed for phase identification and estimation of crystallinity [40].

2.6.4. Scanning Electron Microscopy (SEM) Analysis

SEM was employed to observe the surface morphology of both CuO NPs and nanofibrous scaffolds. The analysis was done using a JSM-IT800 NANO SEM (JEOL, Japan), offering high-resolution imaging for structural evaluation. To improve electron conductivity and image resolution, all specimens were gold-coated before scanning, ensuring clear visualization of fiber texture and nanoparticle distribution [41].

2.6.5. Thermogravimetric Analysis (TGA)

Thermal degradation profiles of the nanofiber scaffolds containing CuO NPs were determined by TGA using a PerkinElmer TGA 8000. Samples weighing around 5 mg were placed in aluminum crucibles and heated from room temperature to 550°C at a rate of 15°C/min. Nitrogen gas was continuously purged to create an inert atmosphere, and real-time mass changes were recorded to evaluate the thermal stability and degradation behavior of the materials [42].

2.6.6. Zeta Potential and Particle Size Analysis

The size and surface charge of the CuO NPs were measured using dynamic light scattering and electrophoretic mobility techniques via the Malvern Zetasizer Ultra. This instrument provided detailed information on the hydrodynamic diameter and zeta potential. The combined analysis offered insights into particle dispersion and colloidal stability, important for assessing performance in biological and material systems [43].

All raw physicochemical characterization data associated with this study are available through Mendeley Data (doi: 10.17632/6tddv74p8k.1).

2.7. Evaluation of antidiabetic activity

2.7.1. α-Amylase Inhibition Assay

The α-amylase inhibitory activity of the test formulations—including algal extract, CuO NPs, and starch/PVA/CuO-NPs nanoscaffolds—was evaluated using a modified version of the dinitrosalicylic acid (DNSA) method [44]. In this assay, 200 µL of α-amylase enzyme solution (1 U/mL) was mixed with 200 µL of each test sample at varying concentrations (25, 50, 75, and 100 µg/mL). This mixture was pre-incubated at 37°C for 10 minutes to allow initial interaction between the enzyme and the sample. After pre-incubation, 200 µL of a 1% starch solution prepared in 0.02 M sodium phosphate buffer (pH 6.9) was added to each tube and incubated again at 37°C for 30 minutes to initiate enzymatic activity. To stop the reaction, 400 µL of DNSA reagent was added, and the tubes were heated in a water bath for 5 minutes to develop a reddish-brown color, which indicates the presence of reducing sugars. The samples were then cooled to room temperature, and the absorbance was measured at 540 nm using a UV–Visible spectrophotometer. Acarbose served as the standard reference drug, and the IC_{50} values of the samples were calculated by plotting inhibition percentages against concentrations using non-linear regression analysis [45].

2.7.2. α-Glucosidase Inhibition Assay

To investigate the α-glucosidase inhibitory activity, a colorimetric assay was performed using p-nitrophenyl-α-D-glucopyranoside (pNPG) as the enzymatic substrate [46]. In this procedure, 50 µL of α-glucosidase enzyme solution (1 U/mL) was combined with 50 µL of the test sample at different concentrations (25, 50, 75, and 100 µg/mL), including the algal extract, CuO NPs, and starch/PVA/CuO-NPs composite. The mixture was incubated at 37°C for 15 minutes to allow enzymatic interaction with the test material. Next, 50 µL of a 5 mM pNPG solution prepared in phosphate buffer (pH 6.8) was added to each tube, and the mixture was further incubated at 37°C for 30 minutes to allow substrate hydrolysis. The enzymatic reaction was terminated by adding 100 µL of 0.1 M sodium carbonate (Na_2CO_3), which facilitated the development of a yellow chromophore due to the release of p-nitrophenol. The absorbance of the resulting solution was measured at 405 nm using a microplate reader [47, 48] . The percentage of enzyme inhibition was calculated using the formula:

Acarbose was used as a positive control, and IC_{50} values were determined through non-linear regression to evaluate the potency of each formulation in inhibiting α-glucosidase activity.

2.8. Statistical analysis

Experimental results were statistically processed using SPSS 25.0 or GraphPad Prism 9.0 software packages. Triplicate measurements were expressed as mean values with standard deviation. Group comparisons employed one-way ANOVA with appropriate post-hoc testing (Tukey's or Dunnett's methods). Statistical significance threshold was established at $p<0.05$. Pearson's coefficient assessed variable correlations, while data normality was verified using Shapiro-Wilk testing. Non-normal distributions underwent logarithmic transformation when required. All conclusions were drawn within a 95% confidence framework to ensure analytical rigor [49].

3. RESULTS

3.1. UV–Visible Spectroscopy

The UV–Visible spectrum (Figure 1) of the macroalgae extract displayed a prominent absorption peak at 267 nm with an absorbance of 0.4035, which is indicative of UV-absorbing phytochemicals such as phenolic compounds or conjugated aromatic systems. The overall absorbance ranged from 0.3285 to 0.4035 between 200–800 nm, with minimal absorption in the visible region (400–700 nm), suggesting a low chlorophyll content, likely due to degradation or purification processes. In comparison, the CuO NP spectrum exhibited a surface plasmon resonance (SPR) peak at 292 nm with a higher absorbance of 0.70716, which is significantly blue-shifted from the typical CuO NP SPR range (570–600 nm). This shift could be attributed to the small particle size, oxidation of the CuO NPs, or interaction with stabilizing agents present during the green synthesis process. The absorbance for CuO NPs ranged from 0.31409 to 0.70716, with a sharp decline after the peak, indicating the formation of monodisperse nanoparticles with minimal aggregation.

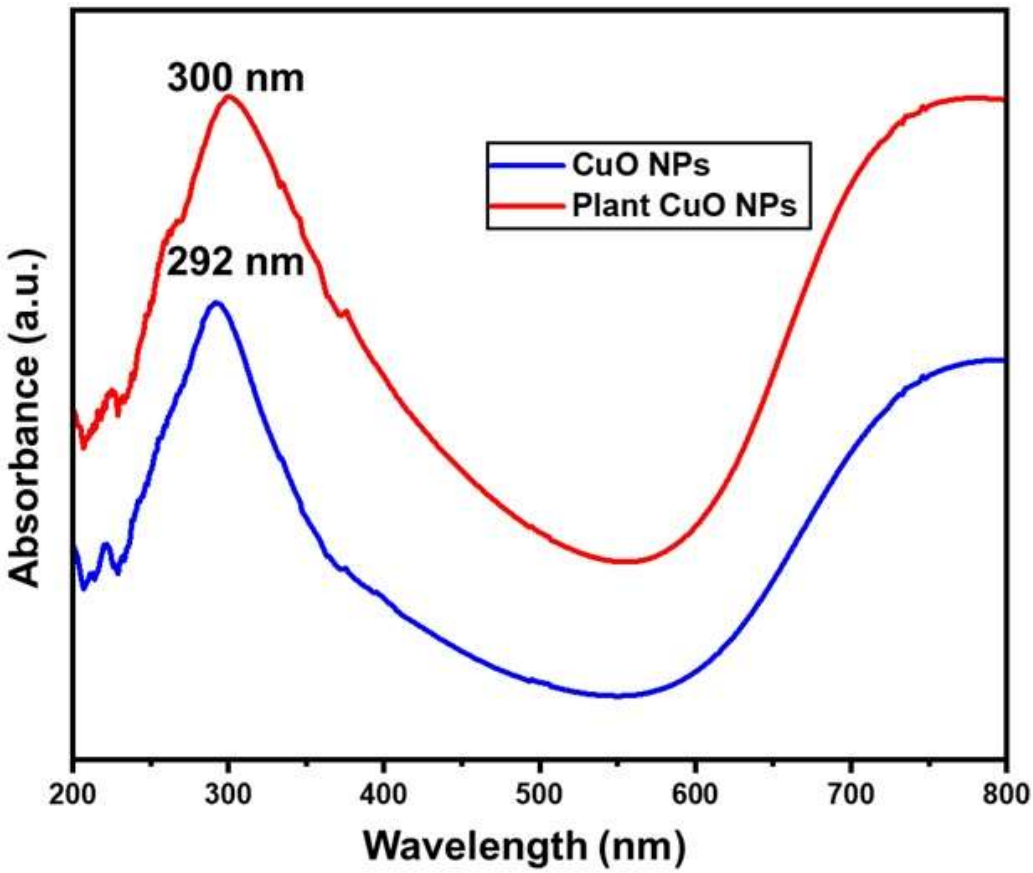

Figure 1: UV–Visible Spectroscopy analysis of algae extract and CuO NPs

3.2. FTIR Spectroscopy

FTIR analysis (Figure 2) of the green-synthesized CuO NPs confirmed the presence of functional groups responsible for nanoparticle formation and stabilization. The spectrum showed a broad peak at 3219.71 cm^{-1}, corresponding to –OH and N–H stretching vibrations, likely derived from phytochemical capping agents. Peaks at 1509.94 cm^{-1} and in the region of 672–463 cm^{-1} were attributed to aromatic ring vibrations and Cu–O stretching, respectively, confirming the formation of CuO NPs. The starch/PVA nanoscaffolds demonstrated characteristic polymeric peaks, including –OH stretching at 3295.71 cm^{-1}, C–H stretching at 2923.65 cm^{-1}, and C–O–C stretching between 1141 and 1088 cm^{-1}. Cu–O peaks overlapping around 605–478 cm^{-1} confirmed successful integration of the nanoparticles into the scaffold. A noticeable shift in the –OH stretching band indicated hydrogen bonding between the CuO NPs and the polymer matrix, which enhanced the scaffold's stability. Additionally, a C=O peak at 1711.09 cm^{-1} was observed, suggesting possible oxidation of PVA or interaction between its carbonyl groups and CuO NPs.

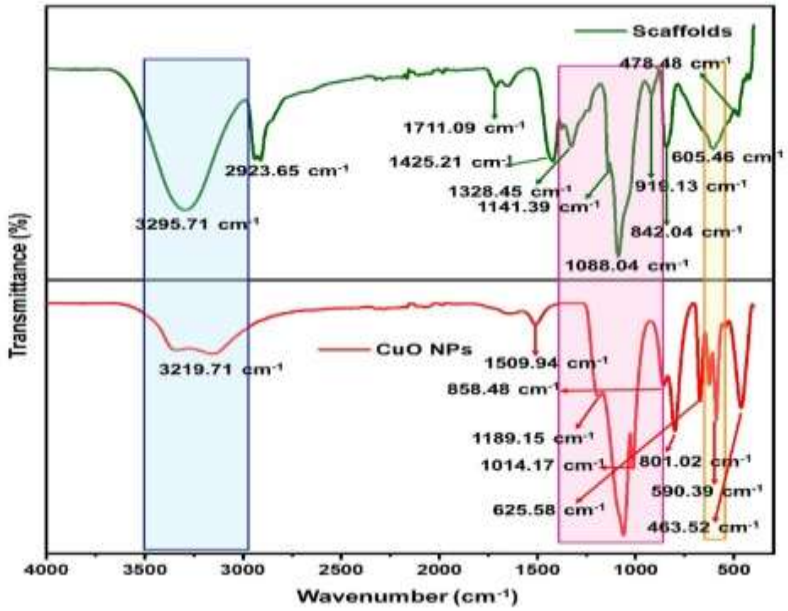

Figure 2: FTIR analysis of CuO NPs and nanoscaffolds

3.3. XRD Analysis

The XRD patterns (Figure 3) of green-synthesized CuO NPs and CuO-loaded starch/PVA nanoscaffolds revealed distinct structural features. The CuO NPs exhibited well-defined peaks at 32.75°, 35.70°, 38.05°, 48.66°, 57.94°, 61.33°, and 75.48° 2θ, with corresponding d-spacings from 1.59 to 3.67 Å, matching the monoclinic crystalline phase of CuO as per JCPDS card no. 48-1548, with no evidence of secondary phases such as Cu_2O. The most intense peak at 35.70° 2θ, corresponding to the (002)/(111) planes, had a net area of 141.86 Cps × °. Scherrer equation-based analysis of peak broadening (FWHM between 0.1°–0.9°) estimated crystallite sizes between 20–50 nm. The starch/PVA nanoscaffolds showed broad diffraction peaks at 21.35°, 22.97°, and 43.14° 2θ, corresponding to the semi-crystalline nature of the polymer matrix, while the reduced intensity CuO peaks at 35.70°, 57.28°, and 61.33° 2θ confirmed the embedded nanoparticles. The broad amorphous hump between 10°–30° 2θ and the reduced FWHM values (0.16°–1.06°) further supported the scaffold's polymer-induced dispersion of CuO NPs. An anomalous negative net intensity at 39.46° 2θ was likely due to instrumental noise or measurement artifacts. Overall, the data validated successful CuO NP synthesis and incorporation into an amorphous nanoscaffold, beneficial for biomedical applications.

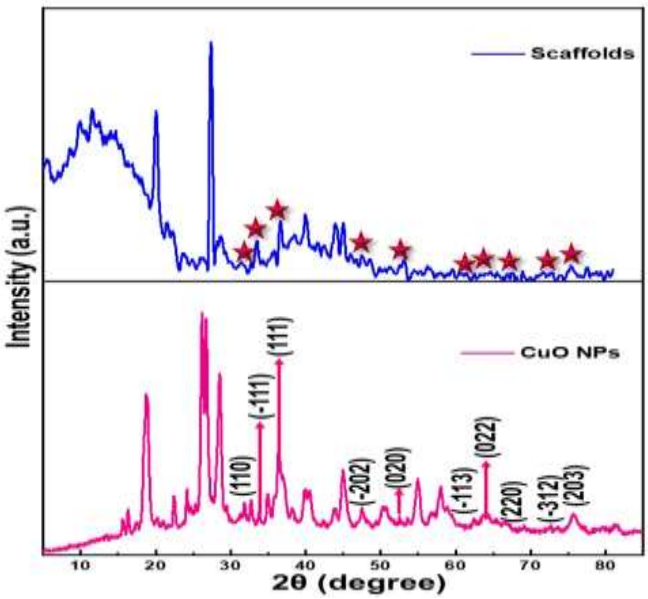

Figure 3: XRD analysis of CuO NPs and nanoscaffolds

3.4. SEM Analysis

SEM images (Figure 4) of the green-synthesized CuO NPs, recorded using a gold-sputtered JSM-IT800 NANO SEM, revealed spherical to irregularly shaped particles in the 50–200 nm size range, with some aggregates reaching 500–1000 nm, likely due to surface charge effects and partial aggregation. The particle surfaces appeared rough, indicating capping by phytochemicals from the macroalgae extract. In contrast, the starch/PVA nanoscaffolds embedded with CuO NPs displayed a well-organized electrospun structure, with uniform, bead-free fibers averaging 150–300 nm in diameter. The scaffolds exhibited a highly porous morphology favorable for biomedical applications such as wound healing and tissue engineering. Bright protrusions of sub-200 nm seen on the nanofiber surfaces represented well-dispersed CuO NPs, confirming successful nanoparticle integration without disrupting the structural integrity or continuity of the fibers.

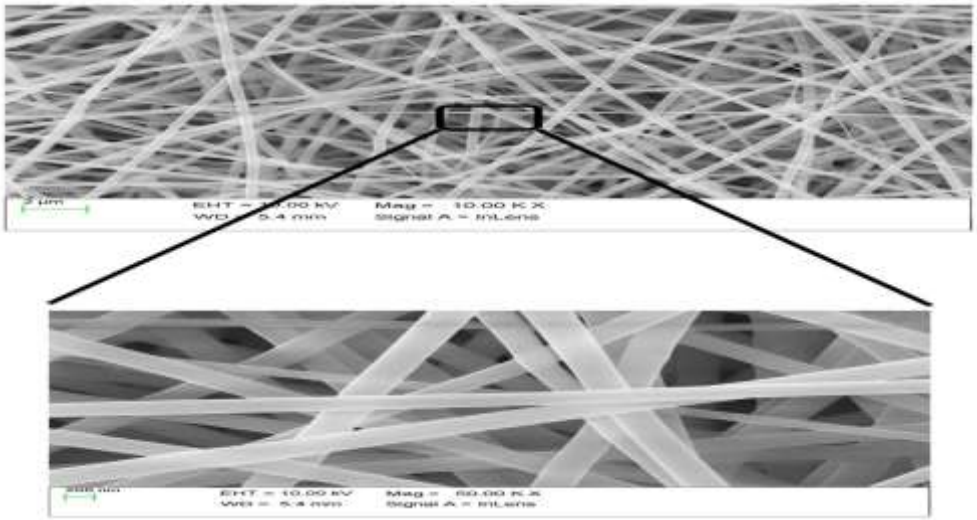

Figure 4: SEM analysis of starch/PVA/CuO-NPs nanoscaffolds

3.5. TGA

Thermal stability of the starch/PVA electrospun nanoscaffolds embedded with CuO NPs was assessed using TGA (Figure 5) under nitrogen atmosphere, where a total mass loss of 35.87% was observed, leaving a residual mass of 64.13%, attributed primarily to the CuO content and other thermally stable components. The degradation profile exhibited three distinct stages: the first stage (50–90°C) corresponded to moisture evaporation with a peak degradation rate of -2.54%/min at 53.71°C; the second and most significant stage (onset at 262.78°C, peak at 326.36°C) showed major decomposition of the starch/PVA polymer backbone involving the cleavage of C–C and C–O bonds, with a degradation rate of -2.93%/min; and the third stage (endset at 363.12°C) represented decomposition of remaining carbonaceous residues. Compared to pure starch/PVA scaffolds, which typically degrade below 250°C, the presence of CuO NPs delayed thermal decomposition and decreased total weight loss, indicating enhanced thermal stability. These thermal properties confirm the scaffold's suitability for biomedical applications requiring sterilization or moderate-temperature processing.

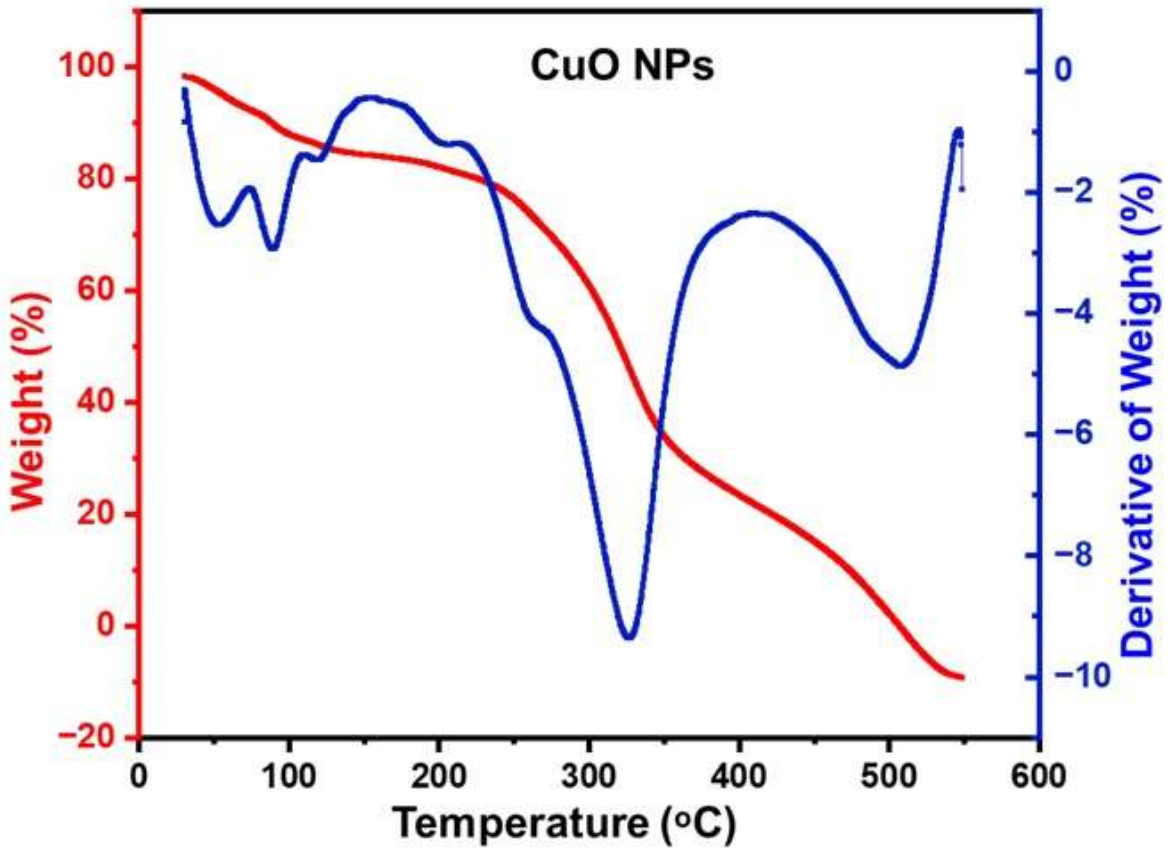

Figure 5: TGA analysis of starch/PVA electrospun nanoscaffolds

3.6. Zeta Potential and Particle Size Analysis

Dynamic Light Scattering analysis of the green-synthesized CuO NPs in aqueous dispersion at 25°C revealed a Z-average hydrodynamic diameter of 125.6 nm (Figure 6) and a polydispersity index (PI) of 0.475, indicating moderate heterogeneity in particle sizes. The size distribution showed three intensity peaks: a dominant population at 881.5 nm (84.89% intensity), a smaller peak at 128.3 nm (12.06%), and a minor aggregation signal at 5350 nm (3.06%) (Figure 7), suggesting partial aggregation among some particles. Electrophoretic Light Scattering (ELS) analysis indicated a zeta potential of -10.03 mV, which is below the ±30 mV threshold for high colloidal stability, implying moderate stability due to limited electrostatic repulsion. Despite the low zeta potential, the presence of phytochemical capping agents likely contributed to some degree of steric stabilization. The measured conductivity was 0.1813 mS/cm, with a dispersant viscosity of 0.887 cP and dielectric constant of 78.5. The quality factor (1.754) and stable phase plots indicated reliable data. However, optimization through surface modification or additional stabilizers may be required to enhance colloidal stability for long-term biomedical use.

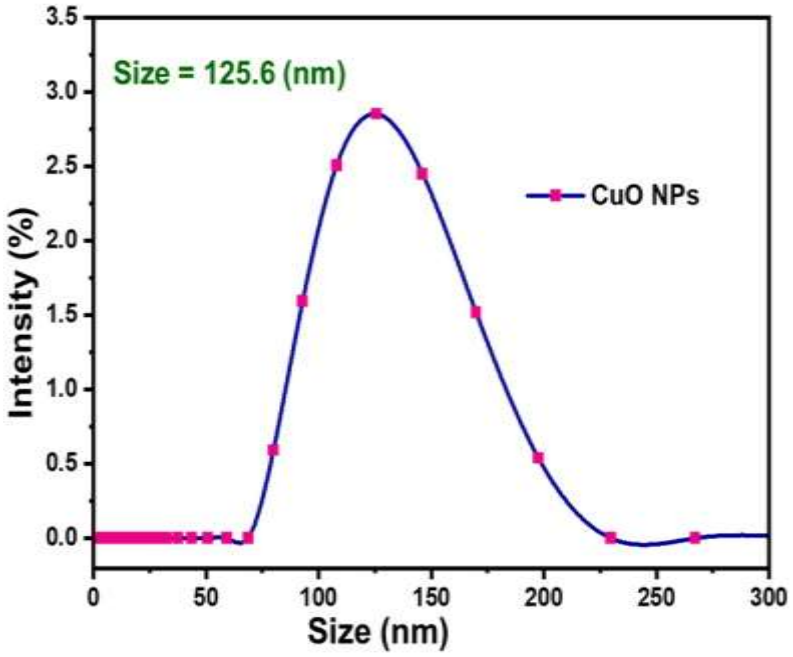

Figure 6: DLS particle size analysis of CuO NPs

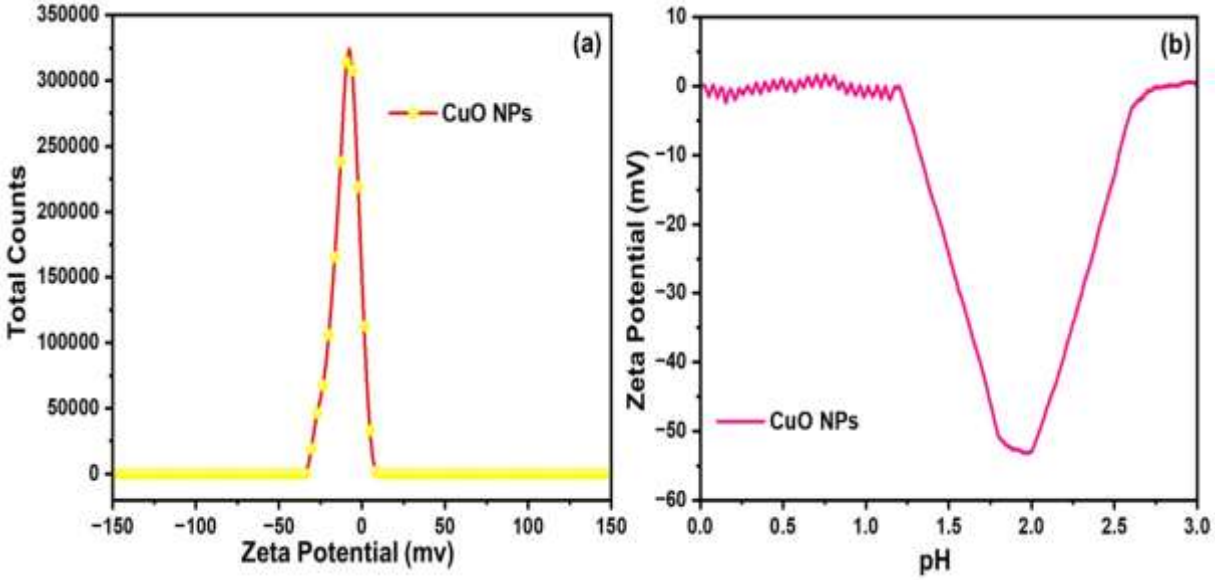

Figure 7: Zeta potential analysis of CuO NPs

3.7. Antidiabetic activity

The antidiabetic activity (Figure 8) of algal extract, CuO NPs, and starch/PVA/CuO-NPs nanoscaffolds was assessed through α-amylase and α-glucosidase inhibition assays. In the α-amylase inhibition assay, the standard (Std) exhibited inhibition percentages of 25.128%, 41.477%, 58.83%, and 81.336% at concentrations of 25, 50, 75, and 100 µg/mL, respectively. The algal extract showed lower inhibition (19.62–54.82%), while CuO NPs demonstrated moderate activity (21.62–69.82%), and the nanoscaffolds exhibited near-standard efficacy (24.62–82.82%). For α-glucosidase inhibition, the standard displayed inhibition percentages of 28.128%, 51.477%, 68.83%, and 84.336% at the same concentrations. The algal extract again showed weaker inhibition (19.62–54.82%), whereas CuO NPs (21.62–69.82%) and nanoscaffolds (27.62–82.82%) performed closer to the standard. These results indicate that nanoscaffolds are the most effective antidiabetic agents, followed by CuO NPs and the algal extract, with significant enzyme inhibition at higher concentrations.

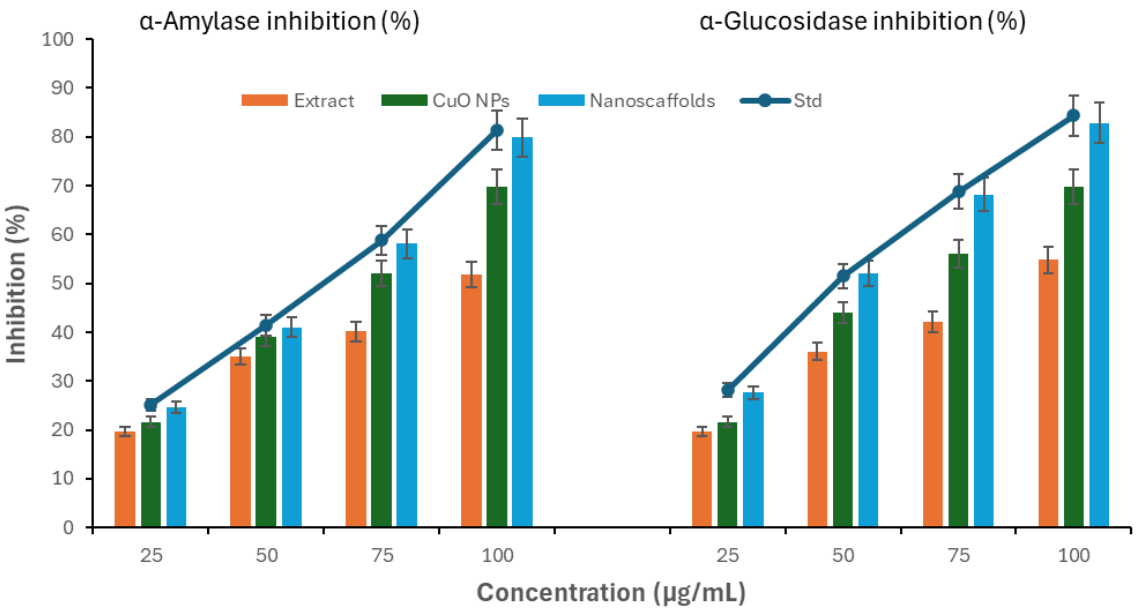

Figure 8: Antidiabetic analysis of algal extract, CuO NPs and starch/PVA/CuO-NPs nanoscaffolds

4. DISCUSSION

The green synthesis of CuO NPs using macroalgal extracts, followed by their integration into starch/PVA nanoscaffolds, demonstrates a promising strategy for developing multifunctional biomaterials with potent antidiabetic potential [50-52]. The characterization techniques employed provided comprehensive insight into the structural, physicochemical, and biological properties of the synthesized materials [53-56].

The UV–visible spectroscopy results revealed distinct absorption behaviors for both the macroalgal extract and the synthesized CuO NPs [57]. The macroalgae extract showed a prominent peak at 267 nm, commonly associated with phenolic compounds and conjugated aromatic systems. This indicates the presence of phytochemicals capable of reducing metal salts and stabilizing nanoparticles [58-60]. The CuO NPs exhibited a surface plasmon resonance (SPR) peak at 292 nm, which is significantly blue-shifted compared to typical metallic Cu NPs. This deviation suggests a smaller particle size and potential oxidation of metallic Cu to CuO, a common outcome in biosynthesis [61]. The sharp absorption decline after the SPR peak indicates monodispersity and reduced aggregation, confirming effective capping and stabilization by algal phytochemicals [62].

FTIR analysis provided further evidence of successful synthesis and integration of CuO NPs into the nanoscaffold. Peaks indicative of hydroxyl and amine groups confirmed the presence of bio-organic functional groups that likely served as capping and stabilizing agents during nanoparticle formation. The emergence of Cu–O vibrational peaks around 463–672 cm^{-1} verified the formation of CuO NPs. In the polymeric starch/PVA matrix, characteristic peaks for –OH, C–H, and C–O–C groups confirmed the structural integrity of the scaffold. Notably, the shift in –OH stretching vibrations suggested hydrogen bonding between CuO NPs and the matrix, implying enhanced interfacial interaction, which could improve mechanical and thermal stability [63, 64].

The XRD analysis revealed well-crystallized monoclinic CuO NPs with no evidence of impurities or secondary phases. The major diffraction peaks corresponded to CuO crystal planes were observed. Upon embedding into the starch/PVA scaffold, a reduction in peak intensity was observed, attributed to nanoparticle dispersion within the polymer matrix. Broad amorphous halos associated with the starch/PVA blend confirmed its semi-crystalline nature, and the presence of key CuO peaks verified successful incorporation without altering the nanoparticle's structural identity [65-67].

SEM imaging offered valuable morphological insights. The green-synthesized CuO NPs displayed a range of shapes from spherical to irregular, with some degree of aggregation possibly resulting from electrostatic interactions and surface energy. However, in the nanoscaffolds, a well-organized, bead-free electrospun fiber morphology was observed. The embedded CuO NPs were visibly dispersed on the nanofiber surface, without compromising fiber continuity. Such a porous architecture, combined with nanoscale fiber dimensions, is highly advantageous for biomedical applications, particularly for wound healing and drug delivery, due to improved cellular attachment and permeability [68].

Thermal stability, evaluated using TGA, confirmed that CuO NP incorporation significantly improved the scaffold's resistance to thermal degradation. While pure starch/PVA scaffolds typically decompose below 250°C, the CuO NP-loaded version maintained structural integrity until around 362°C. This enhancement is attributable to the strong interaction between CuO NPs and the polymer chains, which likely restricts molecular mobility and delays thermal breakdown. The three-stage degradation pattern further reflects distinct loss phases—moisture, polymer decomposition, and residual char combustion—indicating a controlled degradation process [69].

Zeta potential and particle size distribution analyses suggested moderate colloidal stability of the CuO NPs. The hydrodynamic diameter (125.6 nm) and polydispersity index (0.475) indicated a relatively narrow size distribution, albeit

with some degree of aggregation. The observed zeta potential value of –10.03 mV, while lower than the ideal ±30 mV threshold, suggests partial electrostatic repulsion. However, phytochemicals present in the extract likely provided steric stabilization, minimizing aggregation. These properties are crucial for biomedical applications where stability in physiological conditions is essential [70].

In terms of biological activity, the synthesized nanoscaffolds exhibited notable antidiabetic potential [21]. Both α-amylase and α-glucosidase inhibition assays demonstrated that the nanoscaffold formulation outperformed the raw algal extract and CuO NPs alone. While the algal extract exhibited mild inhibition, likely due to phytochemical activity, the CuO NPs showed enhanced enzyme suppression, possibly via oxidative or catalytic interactions with the enzymes [71]. The nanoscaffolds, however, exhibited inhibition levels comparable to the standard drug, especially at higher concentrations, indicating a synergistic effect. The polymeric scaffold may have facilitated sustained release or targeted enzyme interaction, enhancing efficacy. This highlights the potential of the composite scaffold as a natural, biocompatible antidiabetic therapeutic with dual physical and biochemical modes of action [72].

The integration of green-synthesized CuO NPs into starch/PVA nanoscaffolds offers a multifunctional platform with promising thermal stability, structural integrity, and significant antidiabetic activity [10]. The synergistic interaction between phytochemicals, nanoparticles, and polymers appears to enhance bioactivity and material performance, making the formulation highly suitable for future biomedical applications, particularly in controlled drug delivery and diabetic wound care [54].

5. CONCLUSION

This study successfully demonstrated the ultrasonic-assisted green synthesis of CuO NPs using Pocockiella variegata marine macroalgae extract and their subsequent incorporation into starch/PVA electrospun nanoscaffolds for enhanced antidiabetic activity. The biosynthesized CuO NPs exhibited a monoclinic crystalline structure as confirmed by XRD, while FTIR analysis revealed the presence of phytochemical capping agents that stabilized the nanoparticles. SEM imaging showed uniform, bead-free nanofibers (150–300 nm) with well-dispersed CuO NPs, ensuring structural integrity and porosity suitable for biomedical applications. TGA analysis indicated improved thermal stability of the nanoscaffolds due to nanoparticle-polymer interactions, delaying degradation up to 362°C. The antidiabetic evaluation revealed that the CuO NP-loaded nanoscaffolds exhibited superior α-amylase and α-glucosidase inhibition compared to the algal extract and standalone CuO NPs, with efficacy nearing that of the standard drug acarbose. This enhanced activity is attributed to the synergistic effects of phytochemicals, CuO NPs, and the polymeric matrix, which likely facilitate controlled bioactive release. The findings highlight the potential of these eco-friendly nanoscaffolds as a biocompatible, multifunctional platform for diabetes management, offering advantages such as thermal stability, structural robustness, and sustained therapeutic action. Future studies should focus on in vivo validation and optimization for clinical translation.

Ethical Declaration: Not applicable for this study.

Funding: Not available for this study.

Conflicts of Interest: The authors declare no conflicts of interest.

Data Availability Statement: The full dataset of physiochemical characterization associated with this work is published in Mendeley Data [Dataset] Physiochemical characterization of fabricated starch-based nanoscaffolds incorporated with Pocockiella variegata extract-mediated green synthesised copper oxide nanoparticles (DOI: 10.17632/6tddv74p8k.1).
Disclosure: The material characterization data and figures (e.g., UV, SEM, FTIR, XRD, TGA, Zeta Potential and particle sizer) presented here were generated from a common dataset and are being reused across multiple related studies on nanomaterials. All biological analyses and conclusions are original to each manuscript.

REFERENCES

1. Surendran N, Chandrasekaran G, Raju MV, Chandrasekaran MK, Ahalliya RM, Palanisamy CP, Kanniappan GV, Arcot R, Alharbi NS, Thiruvengadam M. Anti-inflammatory potential of ethanolic extract of Maranta arundinacea L.: Insights from COX-2 modulation and oxidative stress analysis. South African Journal of Botany. 2026; 195: 142-151.
2. Pei J, Senthilkumar MV, Hessini K, Subramaniyam S, Sivaramakrishnan R, Kanniappan GV, Jayaraman S, Palanisamy CP. Green fabrication of starch/PVA/CuO nanoscaffolds using marine macroalgae extract for enhanced anti-inflammatory activity. Sustainable Chemistry and Pharmacy. 2026; 51: 102397.
3. Balasubramanian V, Loganathan L, Muthuswamy K, Viswanathan TM, Raju MV, Chandrasekaran MK, Ahalliya RM, Poorasamy J, Palan isamy CP, Dominic S, Kanniappan GV. Anticancer therapeutic efficacy of PEGylated β-galactosidase from Aspergillus terreus in DMBA-induced breast cancer: Toxicological, molecular and histopathological evaluation in Wistar rats. International Journal of Biological Macromolecules. 2026; 360: 151856.
4. Jayaraman S, Eswaran A, Rajagopal P, Palanisamy CP, Veerakumar P, Veeraraghavan VP, Sirasanagandla SR. Neuroendocrine-associated epigenetic factors in cellular senescence: mechanisms and therapeutic implications. Biogerontology. 2026; 27(2): 64.
5. Natarajan SR, Krishnamoorthy R, Alshuniaber MA, Gatasheh MK, Rajagopal P, Veeraraghavan VP, Palanisamy CP, Jayaraman S. KDM1A Facilitates Oncogenic Potential in Colorectal Cancer Progression Through the Activation of AXIN/GSK3β/β-Catenin Signaling Pathways: Evidence From Integrated Transcriptomics and In Vitro Studies. The Journal of Gene Medicine. 2025; 27(11): e70053.

6. Guan T, Gong J, Lin J, Palanisamy CP, Jinjin Pei J, El-Aty AMA. Machine learning-driven multimodal optimization of selenium biotransformation and flavor profiling in fermented apple–Yacon functional beverages. Innovative Food Science & Emerging Technologies. 2025; 105: 104198.
7. Natarajan SR, Krishnamoorthy R, Alshuniaber MA, Alsulami TS, Gatasheh MK, Rajagopal P, Palanisamy CP, Govindan R, Veeraraghavan VP, Jayaraman S. ABCE1 facilitates tumour progression via aerobic glycolysis and inhibits cell death in human colorectal cancer cells through the p53 signalling pathway. Scientific Reports. 2025; 15: 24674.
8. Huang Y, Guo H, Liu Y, Jin W, Palanisamy CP, Pei J, Oz F, El-Aty AMA. Effects of Natural Polysaccharides on the Gut Microbiota Related to Human Metabolic Health. Molecular Nutrition & Food Research. 2025; 69:e202400792.
9. Poornima K, Meenakshi K.C, Manikandan V.R, Shankari G, Prabhu D, Rathi M.A, Palanisamy CP, Balaji R, Gopalakrishnan V.K. Exploring the anticancer potential of Jerantinine A from Tabernaemontana coronaria against prostate, breast, and ovarian cancers: A computational approach. Journal of Complementary and Integrative Medicine, 2025 22(2): 363–372.
10. Palanisamy CP, Poompradub S, Sansanaphongpricha K, Jayaraman S, Subramani K. Faridah Sonsudin gGreen synthesis of Nigella sativa-mediated silver nanoparticles for enhanced antibacterial activity and wound healing: Mechanistic insights and biomedical applications. Environmental Nanotechnology, Monitoring & Management. 2025; 24: 101085.
11. Surendran N, Raju MV, Chandrasekaran MK, Ahalliya RM, Palanisamy CP, Chandrasekaran G, Kanniappan GV. Physicochemical characterization of starch from Maranta arundinacea L.(arrowroot) rhizomes and its inhibition of COX-2: In vivo validation. Bioactive Carbohydrates and Dietary Fibre. 2025; 33: 100465.
12. Kannappan P, Chandrasekaran MK, Raju MV, Gopalakrishnan S, Dhamodharan P, Ahalliya RM, Palanisamy CP, Raju B, Kanniappan GV. Exploring the anticancer potential of Jerantinine A from Tabernaemontana coronaria against prostate, breast, and ovarian cancers: a computational approach. Journal of Complementary and Integrative Medicine. 2025; 22(02): 363-372.
13. Natarajan PM. Dental Bioinformnatics-Current Scope and Future perspectives. Research Journal of Pharmacy and Technology. 2022;15(5):2351-6.
14. Natarajan PM, Umapathy VR, Murali A, Swamikannu B. (2022). Computational Simulations of Identified marine-derived Natural Bioactive Compounds As Potential Inhibitors of Oral Cancer. Future Science OA. 2022; 8(3).
15. Yadalam PK, Chatterjee S, Natarajan PM, Ardila CM. Comparison of light gradient boosting and logistic regression for interactomic hub genes in Porphyromonas gingivalis and Fusobacterium nucleatum-induced periodontitis with Alzheimer's disease. Frontiers in Oral Health. 2025; 6:1463458.
16. Yadalam PK, Natarajan PM, Ardila CM. Variational graph autoencoder for reconstructed transcriptomic data associated with NLRP3 mediated pyroptosis in periodontitis. Scientific Reports. 2025; 15: 1962.
17. Shree P, Sivaramakrishnan R, Kanniappan GV, Pandurangan V, Jayaraman S, Dhayalan VK, Mironescu M, Mironescu ID, Palanisamy CP. Antioxidant and biocompatible CuO-starch/PVA nanoscaffolds via ultrasonic green synthesis using Turbinaria conoides (brown marine macroalgae). Medicine in Drug Discovery. 2025; 28: 100238.
18. Gong J, Lin J, Guan T, Pei J, Palanisamy CP, El-AtyFrom AMA. selenium tolerance to nanoplastic antagonism: Comprehensive characterization of L. casei SNUT1 and its extracellular vesicle–nanoselenium complex. Food Bioscience. 2025; 74: 107749.
19. Poochi SP, Sundarraj R, Raju MV, Chandrasekaran MK, Ahalliya RM, Palanisamy CP, Kanniappan GV, Kondapavuluri BK, Thiruvengadam M. Harnessing Nature: Computational and Experimental Insights Into Ipomoea obscura Metabolites for Bladder Cancer Therapy. Chemistry and Biodiversity. 2025; 0: e00909.
20. Dugganaboyana GK, Kannankumar MKG, Shivaramakrishna S, Raju MV, Chandrasekaran MK, Ahalliya RM, Panneerselvam N, Palanisamy CP, Kanniappan GV. Phytochemical insights, antioxidant activity and therapeutic potential of Cassia senna against prostate cancer in Wistar albino rats. Discover Applied Sciences. 2025; 7:1206.
21. Umapathy V, Dhanavel A, Kesavan R, Natarajan PM, Bhuminathan S, Vijayalakshmi P. Anticancer Potential of the Principal Constituent of Piper nigrum, Piperine: A Comprehensive Review. Cureus. 2024; 16(2): e54425.
22. Umapathy VR, Swamikannu B, Natarajan PM, Devi R, Nandini MS, Vimalarani, Vijayalakshmi P. In Silico Molecular Docking of Ocimum sanctum Phytochemicals: Targeting Key Biomarkers in Oral Cancer. Journal of Pharmacy and Bioallied Sciences. 2024; 16(5): S4792-S4799.

23. Swamikannu B, Umapathy VR, Natarajan PM, Nandini MS, Stylin AGSQ, Vimalarani V, Rajinikanth S. Unlocking the Therapeutic Benefits of Artemisia Annua: A Comprehensive Overview of its Medicinal Properties. Journal of Pharmacy and Bioallied Sciences. 2024; 16(5): S4248-S4253.
24. Yadalam PK, Arumuganainar D, Natarajan PM, Ardila CM. Artificial intelligence-powered prediction of AIM-2 inflammasome sequences using transformers and graph attention networks in periodontal inflammation. Scientific Reports. 2025; 15: 8733.
25. Ponnusamy B, Rajagopal P, Palanisamy CP, Veeraraghavan VP, Jayaraman S. Mechanistic Exploration of the anticancer activity of Justicia adhatoda Plant Leaf Ethanolic Extract against Colon Cancer Cells: An in silico and in vitro Approach. Asian Pacific Journal of Cancer Prevention. 2026; 27(3): 1069-1080.
26. Pei J, Saran VS, Sivaramakrishnan R, Kanniappan GV, Pandurangan V, Jayaraman S, Dhayalan VK, Mironescu M, Mironescu ID, Palanisamy CP. Ultrasonic-assisted, Sargassum ilicifolium (brown marine macroalgae)-mediated biogenic synthesis of CuO nanoparticles incorporated in starch/PVA electrospun nanoscaffolds: In vitro safety and antioxidant efficacy assessment. Bioorganic Chemistry. 2026; 173: 109679.

27. Raj MAPA, Subramaniyam S, Kanniappan GV, Jayaraman S, Palanisamy CP. Sustainable fabrication of starch/PVA/CuO electrospun nanoscaffolds from Turbinaria ornata (marine macroalgae) extract: Physicochemical characterization and antidiabetic evaluation. Kuwait Journal of Science. 2026; 53(2): 100545.
28. Pei J, Ganesh NS, Subramaniyam S, Sivaramakrishnan R, Kanniappan GV, Jayaraman S, Palanisamy CP. Sustainable fabrication of starch/PVA/CuO electrospun nanoscaffolds from Padina tetrastromatica (Brown macroalgae) extract: Physicochemical characterization and antidiabetic assessment. Sustainable Chemistry One World. 2026; 9: 100195.
29. Sakthiraj A, Sivaramakrishnan R, Subramaniyam S, Kanniappan GV, Pandurangan V, Jayaraman S, Dhayalan VK, Mironescu M, Mironescu ID, Palanisamy CP. Chemical Physics Impact. Starch/PVA electrospun nanoscaffolds loaded with ultrasonic-assisted green-synthesis of CuO nanoparticles from marine macroalgae (Gracilaria corticata) extract: Cytotoxicity and antioxidant analysis. 2026; 12: 101018.
30. Raju M, Chandrasekaran MK, Loganathan L, Ahalliya RM, Mironescu M, Mironescu ID, Palanisamy CP, Kanniappan GV. Lipid remodeling and ferroptosis in phosphatidylcholine-mediated tumor–stroma crosstalk. Frontiers in Molecular Biosciences. 2026; 13: 1742305.
31. Kunamalla R, Panagal M, Palanisamy CP. Biogenic synthesis and fabrication of starch/PVA/CuO electrospun nanoscaffolds from Sargassum ilicifolium (brown marine macroalgae) extract for anticancer activity on HT-29 and MCF-7 cancer cells. Biocatalysis and Agricultural Biotechnology. 2026; 72: 103923.
32. Pei J, Govindaraj H, Sivaramakrishnan R, Kanniappan GV, Pandurangan V, Dhayalan VK, Mironescu M, Mironescu ID, Jayaraman S, Palanisamy PC. Sustainable fabrication of biopolymer-based (starch/PVA) nanoscaffolds loaded with green-synthesized CuO nanoparticles from Sargassum wightii (marine macroalgae): Cytocompatibility and antioxidant activity. Biomaterials Advances. 2026; 182: 214660.
33. Pei J, Perumal NC, Meng P, Long Q, Palanisamy CP. Extracellular vesicle-based biosensors for Alzheimer's disease: A new frontier in precision diagnostics. Ageing Research Reviews. 2026; 113: 102904.
34. Umapathy VR, Natarajan PM, Swamikannu B. Regenerative Strategies in Dentistry: Harnessing Stem Cells, Biomaterials and Bioactive Materials for Tissue Repair. Biomolecules. 2025; 15: 546.
35. Ganesan A, Kumar NG, Natarajan PM. Solanum trilobatum leaf extract-derived silver nanoparticles downregulate the PI3K/AKT/mTOR signaling pathway and attenuate oral squamous cell carcinoma cell proliferation. Journal of Herbmed Pharmacology. 2024; 13(2): 300-307.
36. Perumal MKK, Renuka RR, Subbiah SK, Natarajan PM. Artificial intelligence-driven clinical decision support systems for early detection and precision therapy in oral cancer: a mini review. Frontiers in Oral Health. 2025; 6: 1592428.
37. Ramesh E, Ganesan A, Lakshmi KC, Natarajan PM. Artificial intelligence-based diagnosis of oral leukoplakia using deep convolutional neural networks Xception and MobileNet-v2. Frontiers in Oral Health. 2025; 6: 1414524.
38. Ganesan A, Kumar NG, Natarajan PM. Anticancer activity of silver nanoparticles synthesized from aqueous leaf extract of Solanum trilobatum (Purple fruit pea eggplant) on human oral cancer cells. Journal of Herbmed Pharmacololgy. 2024; 13(2): 260-268.
39. Pei J, Kumarasamy RV, Jayaraman S, Kanniappan GV, Long Q, Palanisamy CP. Quercetin-functionalized nanomaterials: Innovative therapeutic avenues for Alzheimer's disease management. Ageing Research Reviews. 2025; 104: 102665.
40. Jayaraman S, Prasad M, Natarajan SR, Krishnamoorthy R, Alshuniaber MA, Gatasheh MK, Veeraraghavan VP, Rajagopal P, Palanisamy CP. Molecular mechanisms underlying the effects of beta-sitosterol on TGF-β1/Nrf2/SIRT1/p53-mediated signaling in the kidney of a high-fat diet and sucrose-induced type-2 diabetic rat. Chemico-Biological Interactions. 2025; 411: 111443.
41. Huang Y, Guo H, Liu Y, Jin W, Palanisamy CP, Pei J, Oz F, El-Aty AMA. Effects of Natural Polysaccharides on the Gut Microbiota Related to Human Metabolic Health. Molecular Nutrition & Food Research. 2025; e202400792.
42. Prabhakaran P, Palanisamy CP, Shanmugam A, Damodharan P, Swaminathan H, Devaraj D, Ahalliya RM, Kanniappan GV. Isolation, structural characterization, and molecular docking studies on the bioactive compound from n-Hexane extract of Emilia sonchifolia (L.) DC against the pancreatic cancer target Aurora 2 Kinase. Journal of Complementary and Integrative Medicine. 2024; 22(1): 0290.
43. Jiang H, Kumarasamy RV, Pei J, Raju K, Kanniappan GV, Palanisamy CP. Integrating engineered nanomaterials with extracellular vesicles: Advancing targeted drug delivery and biomedical applications. Frontiers in Nanotechnology. 2024; 6: 1513683.
44. Guo H, Liu Y, Wan T, Song D, Palanisamy CP, Geng J, Pei J, Özmen S, El-Aty AMA. Toward personalized cancer management: Role of precision nutrition–diet interventions. Journal of Functional Foods. 2024; 123: 106584.
45. Natarajan SR, Krishnamoorthy R, Alshuniaber MA, Al-Anazi KM, Farah MA, Rajagopal P, Palanisamy CP, Veeraraghavan VP, Jayaraman S. Identification of FOXM1 as a novel protein biomarker and therapeutic target for colorectal cancer progression: Evidence from immune infiltration and bioinformatic analyses. International Journal of Biological Macromolecules. 282 (Part 4): 137201.
46. Rajendran MS, Jayaraman S, Khan JM, Jasmine S, Prabhakaran RK, Raju MV, Chandrasekaran MK, Ahalliya RM, Kannappan P, Palanisamy CP, Kanniappan GV. Investigating the colon toxicity and carcinogenic role of monosodium glutamate compared with Dimethylhydrazine in male Wistar rats: Exploring the link to childhood colon cancer risk. Journal of King Saud University - Science. 2024; 36(11): 103507.
47. Natarajan PM, Umapathy VR. Role of transcriptomics in the study of oral cancer. Frontiers in Oral Health. 2025; 6:1524364.
48. Natarajan PM, Swamikannu B, Sivaraman NM, Stylin AGSQ. Prevention of Oral Cancer: A Comprehensive Guide. Journal of Pharmacy and Bioallied Sciences. 2024; 16(5): S4239-S4241.

49. Natarajan PM. Computational Studies on Recent Congeners of Fluoroquinolones and Nitroimidazoles for Their Use in Periodontal Therapy. Journal of Pharmacy and Bioallied Sciences. 2024; 16(5): S4731-S4740.
50. Natarajan PM, Bhuminathan S, Rajan R, Bindu K, Loganathan K, Veerakumar R. The Crucial Role of Smoking Cessation in Preventing Oral Cancer. Journal of Pharmacy and Bioallied Sciences. 2024; 16(5): S4245-S4247.
51. Natarajan PM, Bhuminathan S, Leela B, Bindu K, Loganathan K, Ramachandran V. Smoking and its Role in Oral Cancer. Journal of Pharmacy and Bioallied Sciences 16(5): S4242-S4244.
52. Vidhyarekha U, Natarajan PM, Bhuminathan S, Sabarinathan J, Suba R, Vijayalakshmi P. Role of artificial intelligence in Oral Cancer. Advances in Public Health. 2024. 2024: 3664408.
53. Ganesan A, Kumar NG, Natarajan PM, Gauthaman J. Automated classification of elongated styloid processes using deep learning models-an artificial intelligence diagnostics. Frontiers in Oral Health. 2025; 5: 1424840.
54. Pei JJ, Yan Y, Palanisamy CP, Jayaraman S, Natarajan PM, Umapathy VR, Gopathy S, Roy JR, Sadagopan JC, Thalamati D, Mironescu M. Materials-based drug delivery approaches: Recent advances and future perspectives. Green Processing and Synthesis. 2024; 13: 20230094.
55. Panneerselvam S, Viswaja K, Deepa E, Prathiba S, Rebecca FS, Nivedha RP, Rajagopal P, Veeraraghavan VP, Sridevi G, Palanisamy CP, Jayaraman S. Hypoglycemic Potential of Acalypha indica in Streptozotocin-Induced Type 2 Diabetic Rats. International Journal of Drug Delivery Technology. 2026; 16(26s):1038-1047.
56. Panneerselvam S, Viswaja K, Prathiba S, Rebecca FS, Nivedha RP, Rajagopal P, Fathima SJH, Veeraraghavan VP, Sridevi G, Palanisamy CP, Jayaraman S. Acalypha Indica Attenuates Insulin Resistance in STZ-Induced Type 2 Diabetic Male Rats: Mechanistic Study. International Journal of Drug Delivery Technology. 2026; 16(26s):1027-1037.
57. Manju NE, Natarajan A, Rebecca FS, Nivedha RP, Hemalatha R, Rajagopal P, Murali R, Veeraraghavan VP, Sridevi G, Palanisamy CP, Jayaraman S. Effect of Seendhil polyherbal formulation in attenuating type-2 diabetes in STZ-induced experimental rats. International Journal of Drug Delivery Technology. 2026; 16(26s):981-989.
58. Manju NE, Natarajan A, Rebecca FS, Nivedha RP, Hemalatha R, Rajagopal P, Murali R, Veeraraghavan VP, Sridevi G, Palanisamy CP, Jayaraman S. Molecular mechanism to identify the effects of Seendhil polyherbal preparation on IRS-1/AKT/GLUT4/NRF2-KEAP-1 mediated signaling in SFZ-induced type-2 diabetic adult male rats. International Journal of Drug Delivery Technology. 2026;16(26s):972-980.
59. Palanisamy CP, Poompradub S, Sansanaphongpricha K, Jayaraman S, Subramani K, Sonsudin F. Biosynthesis of silver nanoparticles (AgNPs) using ethanolic extract of Nigella sativa (L.) seeds promotes wound healing via PDGF and VEGF signalling pathways activation. Biocatalysis and Agricultural Biotechnology. 2023; 54: 102970.
60. Palanisamy CP, Pei JJ, Phaniendra A, Venkata AAN, Jayaraman S, Veeraragahavan VP, Sridevi G, Roy JR, Janaki CS, Thalamati D, Mironescu M, Luo Q, Chai Y, Long Q. New Strategy of Neurodegenerative Disease Treatment with Extracellular Vesicles (EVs) Derived from Mesenchymal Stem Cells (MSCs). Theranostics. 2023; 13(12):4138-4165.
61. Kumarasamy RV, Natarajan PM, Umapathy VR, Roy JR, Rab SO, Saeed M, Panagal M, Mironescu M, Srinivasan GP, Palanisamy CP. Clinical Applications and Therapeutic Potentials of Advanced Nanoparticles: A Comprehensive Review on Completed Human Clinical Trials. Frontiers in Nanotechnology. 2024; 6:1479993.
62. Jin W, Pei JJ, Roy JR, Jayaraman S, Ahalliya RM, Kanniappan GV, Mironescu M, Palanisamy CP. Comprehensive review on single-cell RNA sequencing: A new frontier in Alzheimer's disease research. Ageing Research Reviews. 2024; 274: 102454.
63. Pei J, Palanisamy CP, Jayaraman S, Natarajan PM, Umapathy VR, Roy JR, Panagal M, Jayaraman S. Curcumin-loaded polymeric nanomaterials as a novel therapeutic strategy for Alzheimer's disease: A comprehensive review. Ageing Research Reviews. 2024; 99: 102393.
64. Pei J, Palanisamy CP, Jayaraman S, Natarajan PM, Umapathy VR, Roy JR, Thalamati D, Ahalliya RM, Kanniappan GV*, Mironescu M. A comprehensive review on starch-based Sustainable Edible Films Loaded with Bioactive Components for Food Packaging. International Journal of Biological macromolecules. 2024; 274 (Part-1): 133332.
65. Palanisamy CP, poompradub S, Sansanaphongpricha K, Subramani K, Sonsudin F. Increased expression levels of PDGF and VEGF magnify the wound healing potential facilitated by biogenic synthesis of silver nanoparticles. Nano-Structures & Nano-Objects. 2024; 39: 101236.
66. Pei J, Palanisamy CP, Jayaraman S, Natarajan PM, Umapathy VR, Roy JR, Thalamati D, Ahalliya RM, Kanniappan GV, Mironescu M. Proteomics Profiling of Extracellular Vesicle for Identification of Potential Biomarkers in Alzheimer's Disease: A Comprehensive Review. Ageing Research Reviews. 2024; 99: 102359.
67. Xi J, Wang T, Xian P, Liu X, Du M, Yang H, Palanisamy CP, Lin W, Long Q. Proteomic insights uncover enhanced neurotherapeutic potential in conditioned mesenchymal stem cell-derived extracellular vesicles. Extracellular Vesicle. 2024; 3: 100037.
68. Pei J, Natarajan PM, Umapathy VR, Swamikannu B, Sivaraman NM, Krishnasamy L, Palanisamy CP. Advancements in the synthesis and functionalization of zinc oxide-based nanomaterials for enhanced oral cancer therapy. Molecules. 2024; 29(11): 2706.
69. Gatasheh MK, Natarajan SR, Krishnamoorthy R, Alsulami TS, Rajagopal P, Palanisamy CP, Veeraraghavan VP, Jayaraman S. Molecular analysis to identify novel potential biomarkers as drug targets in colorectal cancer therapy: an integrated bioinformatics analysis. Molecular and Cellular Oncology. 2024; 11(1): 2326699.
70. Pei J, Yan Y, Jayaraman S, Rajagopal P, Natarajan PM, Umapathy VR, Gopathy S, Roy JR, Sadagopan CS, Thalamati D, Palanisamy CP, Mironescu M. A review on advancements in the application of starch-based nanomaterials in biomedicine: Precision drug delivery and cancer therapy. International Journal of Biological Macromolecules. 2024; 130746.

71. Tiwari P. Recent trends in therapeutic approaches for diabetes management: a comprehensive update. Journal of diabetes research. 2015;2015(1):340838.
72. Zahin N, Anwar R, Tewari D, Kabir MT, Sajid A, Mathew B, et al. Nanoparticles and its biomedical applications in health and diseases: special focus on drug delivery. Environmental Science and Pollution Research. 2020;27(16):19151-68.